Check for updates

Efficient degradation of organic pollutants by peroxymonosulfate activated with MgCuFe-layered double hydroxide†

Jianyao Zhu,[ac] Zhiliang Zhu, [ID] *[ac] Hua Zhang,[a] Hongtao Lu[a] and Yanling Qiu[bc]

In this study, MgCuFe-layered double hydroxide (MgCuFe-LDH) was for the first time used as a catalyst for peroxymonosulfate (PMS) activation towards the degradation of aqueous organic pollutants. Compared with both MgFe-LDH and MgCuAl-LDH materials, MgCuFe-LDH exhibited significantly higher catalytic activity to activate PMS for the degradation of acetaminophen. The effects of catalyst loading, PMS dosage, reaction temperature and initial solution pH on the degradation efficiency of acetaminophen were investigated. Acetaminophen (5 mg L^{-1}) degradation at about 93.0% was achieved at 20 min by using 0.3 g L^{-1} MgCuFe-LDH and 0.5 mM PMS. Under the same conditions, rhodamine B (RhB, 5 mg L^{-1}) can be almost completely decolorized (99.5%) within 45 min. Radical scavenger and electron paramagnetic resonance (EPR) experiments showed that sulfate radicals (SO$_4^{\bullet-}$) and hydroxyl radicals (·OH) existed in PMS/MgCuFe-LDH system. The generated radicals played vital roles in the catalytic degradation of organic pollutants. A possible activation mechanism of PMS on MgCuFe-LDH was put forward. This study indicates that MgCuFe-LDH is a promising catalyst to activate PMS for the efficient degradation of organic pollutants.

1. Introduction

In recent decades, organic pollutants like pharmaceuticals and dyes in the aquatic environment have received considerable attention due to their adverse effects on the ecosystem and human health. Tremendous efforts have been made to develop advanced technologies for the remediation of contaminated water. At present, the use of advanced oxidation processes (AOPs) has become one of the most promising approaches for the elimination of organic pollutants from water. Among them, the sulfate radical (SO$_4^{\bullet-}$)-based AOP has been suggested as an effective way to degrade hazardous organic pollutants in aqueous media. Due to its high redox potential, SO$_4^{\bullet-}$ is able to react with a broad range of organic pollutants.[1–5] Generally, SO$_4^{\bullet-}$ is generated *via* peroxydisulfate (PDS) or peroxymonosulfate (PMS) activation. The PMS is usually activated by transition metals more easily than PDS.[6] Transition metals such as Fe, Co, Cu and Mn have been applied as the catalysts of PMS

activation and displayed high catalytic activity for organic pollutants degradation.[7–13]

Layered double hydroxide (LDH), made up of positively charged metal hydroxide layers and interlayer negatively charged anions, is a kind of multi-metal clay material. The LDH has a general formula of $[M_{1-x}^{2+}M_x^{3+}(OH)_2]^{x+}(A^{n-})_{x/n}\cdot mH_2O$, where M^{2+} is divalent metal cations, M^{3+} is trivalent metal cations, A^{n-} denotes interlayer inorganic or organic anion with a negative charge n, m is water molecule number in the interlayer, and x is M^{3+}/(M^{2+} + M^{3+}) ratio and normally between 0.2–0.4. In the past decade, LDH materials have received much attention as electrode materials,[14–17] adsorbents[18–21] and catalysts/catalyst precursors[22–26] because of their unique physical and chemical properties.

Although the advances have been achieved for LDH, there are still very limited reports on LDH as a catalyst of PMS activation. In our previous report, we have demonstrated that MgCuFe-LDH is an efficient adsorbent for arsenate removal from water.[19] In this work, we report that MgCuFe-LDH was used as an efficient catalyst for the activation of PMS towards organic pollutants degradation. As one of the most common pharmaceuticals, acetaminophen (Fig. 1) was chosen as a model contaminant. The MgCuFe-LDH exhibited much higher catalytic activity than both MgFe-LDH and MgCuAl-LDH. The catalytic activity of MgCuFe-LDH in PMS activation was also evaluated using organic dye rhodamine B (RhB, Fig. 1) as another model contaminant. In addition, the possible activation mechanism of PMS on MgCuFe-LDH was put forward. This

[a]State Key Laboratory of Pollution Control and Resource Reuse, Tongji University, Shanghai 200092, China. E-mail: zzl@tongji.edu.cn

[b]Key Laboratory of Yangtze River Water Environment, Ministry of Education, Tongji University, Shanghai 200092, China

[c]Shanghai Institute of Pollution Control and Ecological Security, Shanghai 200092, China

† Electronic supplementary information (ESI) available. See DOI: 10.1039/c8ra09841g

study may provide a new perspective for the decontamination of polluted water based on MgCuFe-LDH material and expand the application of MgCuFe-LDH from adsorption to catalysis.

2. Experimental section

2.1 Preparation of LDH materials

A constant pH co-precipitation method was used to synthesize MgCuFe-LDH.[27] Briefly, a solution containing $Mg(NO_3)_2 \cdot 6H_2O$ (48 mmol), $Cu(NO_3)_2 \cdot 3H_2O$ (12 mmol) and $Fe(NO_3)_3 \cdot 9H_2O$ (20 mmol) was prepared in 100 mL ultrapure water. Another solution was made by dissolving NaOH (1 mol L^{-1}) and Na_2CO_3 (2 mol L^{-1}) in ultrapure water. Subsequently, the above two solutions were added drop by drop into 100 mL of ultrapure water under energetic magnetic stirring. During the reaction process, the pH of solution was maintained at about 10.5. The resulting slurry was heated and kept at 353 K for 24 h in an oven. After cooling, the product was collected by filtration. Finally, the obtained material was washed with ultrapure water for three times and dried at 333 K. For comparison, MgFe-LDH ($Mg(NO_3)_2 \cdot 6H_2O$ (60 mmol) and $Fe(NO_3)_3 \cdot 9H_2O$ (20 mmol)) and MgCuAl-LDH ($Mg(NO_3)_2 \cdot 6H_2O$ (48 mmol), $Cu(NO_3)_2 \cdot 3H_2O$ (12 mmol) and $Al(NO_3)_3 \cdot 9H_2O$ (20 mmol)) were also prepared by the same method.

2.2 Characterization

The metal contents of the prepared LDH materials were determined by an inductively coupled plasma optical emission spectrometer (ICP-OES, Agilent 720-ES, USA) after the samples were dissolved in nitric acid. X-ray diffraction (XRD) patterns were acquired using a German Bruker D8 Advance X-ray diffractometer with Cu Kα radiation (40 kV, 40 mA). Fourier transform infrared (FTIR) spectroscopy was performed on a Thermo Fisher Scientific Nicolet 5700 FTIR spectrometer (USA) in the range 4000–400 cm^{-1}. Morphology, metal elemental composition and mapping were analyzed with a field-emission scanning electron microscope (FE-SEM, Zeiss Supra 55, Germany) equipped with an energy dispersive X-ray (EDX, Oxford Instruments, UK) analyzing system and a transmission electron microscope (TEM, Hitachi HT7700, Japan). The N_2 adsorption–desorption isotherms of LDH materials were obtained at 77 K using an Autosorb iQ analyzer (Quantachrome Instruments, USA). The Brunauer–Emmett–Teller (BET) method was employed to calculate the specific surface areas. The X-ray photoelectron spectroscopy (XPS) analysis of materials was performed using an Escalab 250Xi instrument (Thermo Fisher Scientific, USA) with Al Kα radiation. The binding energies were referenced to the C 1s line at 284.8 eV from adventitious carbon. Electron paramagnetic resonance (EPR) experiment was conducted on a German Bruker Elexsys spectrometer using 5,5-dimethyl-1-pyrroline N-oxide (DMPO) as a radical spin trapping agent.

2.3 Catalytic activity experiments

The catalytic performances of LDH materials were tested and evaluated for the activation of PMS (available as Oxone®
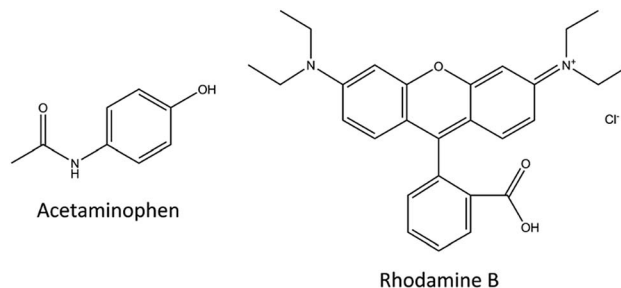

Fig. 1 Chemical structures of acetaminophen and rhodamine B.

($KHSO_5 \cdot 0.5KHSO_4 \cdot 0.5K_2SO_4$)) towards acetaminophen or RhB degradation. The catalytic activity experiments were carried out in a beaker containing 100 mL of 5 mg L^{-1} acetaminophen or 5 mg L^{-1} RhB, 0.3 g L^{-1} LDH and 0.5 mM PMS at 25 °C, unless otherwise specified. During the reaction process, the mixture was continuously stirred. At preplanned time intervals, an aliquot of the reaction solution was taken out and filtered with a 0.45 μm membrane filter. Then acetaminophen in the obtained solution was detected by an ultra-performance liquid chromatography system coupled with a photodiode array detector (UPLC-PDA, Waters Acquity I-class, USA). The RhB in the solution was analyzed on a UV-vis spectrophotometer (UV-3200PC, Mapada Instruments, China) at 554 nm wavelength. Total organic carbon (TOC) analysis was conducted on a TOC analyzer (TOC-L, Shimadzu, Japan). The concentrations of leaching metal ions were determined by ICP-OES.

3. Results and discussion

3.1 Characterization of materials

The chemical analysis results of MgCuFe-LDH, MgCuAl-LDH and MgFe-LDH are summarized in Table 1. It can be found that the metal molar ratios of MgCuFe-LDH, MgCuAl-LDH and MgFe-LDH are close to that of the starting salts, respectively.

Fig. 2a illustrates the XRD patterns of MgCuFe-LDH, MgCuAl-LDH and MgFe-LDH, respectively. All of the three samples exhibited pretty similar XRD patterns and displayed the characteristic diffraction peaks of typical LDH materials. The (003) spacing of MgCuFe-LDH, MgCuAl-LDH, and MgFe-LDH were calculated to be ~0.770, ~0.767 and ~0.773 nm, respectively, which are consistent with the value of LDH with carbonate intercalation reported in previous studies.[27,28]
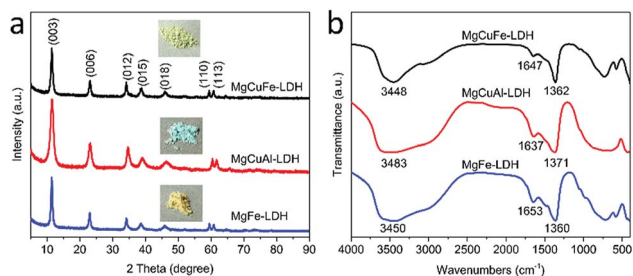
The FTIR spectra of MgCuFe-LDH, MgCuAl-LDH and MgFe-LDH (Fig. 2b) are very similar. The broad bands at about 3448, 3483 and 3450 cm^{-1} are the O–H stretching vibration of hydroxyl groups in LDH layers and interlayer H_2O molecules. The bands at 1647, 1637 and 1653 cm^{-1} are characteristic of the bending vibration of interlayer H_2O. The appearance of intense bands at 1362, 1371 and 1360 cm^{-1} are the ν_3 (asymmetric stretching) mode of CO_3^{2-}, indicating the existence of CO_3^{2-} ions in the interlayer of LDH. In addition, the bands below 1000 cm^{-1} result from the lattice vibrations of M–O and M–OH (M represents Mg, Cu, Fe and Al).

The N_2 adsorption–desorption isotherms of MgCuFe-LDH, MgCuAl-LDH and MgFe-LDH are displayed in Fig. 3. The N_2
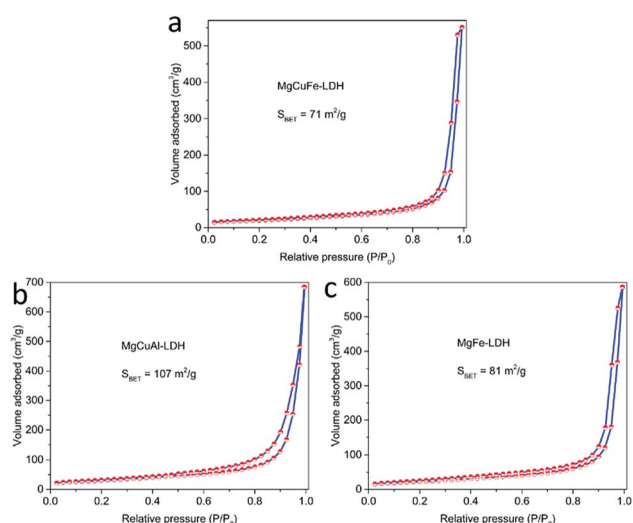
Table 1 Chemical analysis of MgCuFe-LDH, MgCuAl-LDH and MgFe-LDH

Materials	Metal molar ratio of starting salts	Metal molar ratio of LDH	Chemical composition
MgCuFe-LDH	Mg : Cu : Fe = 2.4 : 0.6 : 1	Mg : Cu : Fe = 2.31 : 0.56 : 1	$[Mg_{0.597}Cu_{0.145}Fe_{0.258}(OH)_2]^{0.258+}$ $(CO_3{}^{2-})_{0.129} \cdot mH_2O$
MgCuAl-LDH	Mg : Cu : Al = 2.4 : 0.6 : 1	Mg : Cu : Al = 2.37 : 0.61 : 1	$[Mg_{0.596}Cu_{0.153}Al_{0.251}(OH)_2]^{0.251+}$ $(CO_3{}^{2-})_{0.1255} \cdot mH_2O$
MgFe-LDH	Mg : Fe = 3 : 1	Mg : Fe = 2.55 : 1	$[Mg_{0.718}Fe_{0.282}(OH)_2]^{0.282+}(CO_3{}^{2-})_{0.141} \cdot mH_2O$
MgCuFe-LDH after three runs	Mg : Cu : Fe = 2.4 : 0.6 : 1	Mg : Cu : Fe = 1.31 : 0.46 : 1	$[Mg_{0.473}Cu_{0.166}Fe_{0.361}(OH)_2]^{0.361+}$ $(CO_3{}^{2-})_{0.1805} \cdot mH_2O$

Fig. 2 (a) XRD patterns and (b) FTIR spectra of MgCuFe-LDH, MgCuAl-LDH and MgFe-LDH.

adsorption–desorption isotherm curves of samples exhibit a type IV isotherm with H3-type hysteresis loop in the IUPAC classification. This type of hysteresis loop does not show any limiting adsorption at high P/P₀ region, which is commonly ascribed to the aggregates of plate-like particles resulting in slit-shaped pores.[29] The specific surface areas calculated by BET method were 71, 107 and 81 m² g⁻¹ for MgCuFe-LDH, MgCuAl-LDH and MgFe-LDH, respectively. The BET surface areas of LDH materials are higher than those of the reported metal oxide and spinel-type catalysts.[7,9–11,13] The higher specific surface area is expected to provide more active sites for catalysis.

SEM and TEM were used to observe the microstructure of MgCuFe-LDH. As revealed in Fig. 4, the SEM and TEM images of MgCuFe-LDH exhibit a lamellar structure.

In the EDX spectrum of MgCuFe-LDH (Fig. 5a), the metal elemental peaks of Mg, Cu and Fe can be observed. The EDX analysis shows that the Mg/Cu/Fe molar ratio of MgCuFe-LDH is 2.72 : 0.69 : 1, which is close to the value obtained from ICP-OES. Furthermore, the distribution of metal elements in MgCuFe-LDH was investigated by EDX mapping analysis under SEM observation (Fig. 5b). The images visualized the presence and uniform distribution of Mg, Cu and Fe elements.

The chemical composition of MgCuFe-LDH was determined by XPS. As presented in Fig. 6a, the full XPS spectrum of MgCuFe-LDH reveals the presence of C, O, Mg, Cu and Fe. The high-resolution XPS spectrum for C 1s is given in Fig. 6b. The presence of C 1s peak at 288.9 eV is contributed by the interlayer carbonate groups of LDH material.[30] The high-resolution XPS
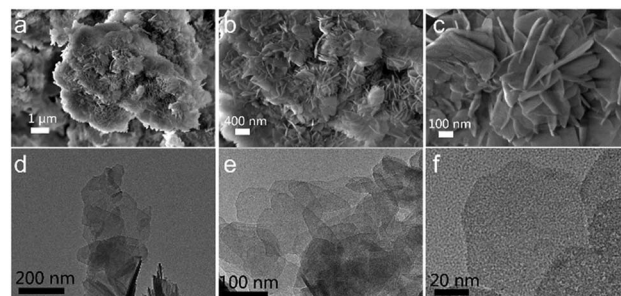
Fig. 4 (a–c) SEM and (d–f) TEM images of MgCuFe-LDH.

Fig. 3 N₂ adsorption–desorption isotherms of (a) MgCuFe-LDH, (b) MgCuAl-LDH and (c) MgFe-LDH.
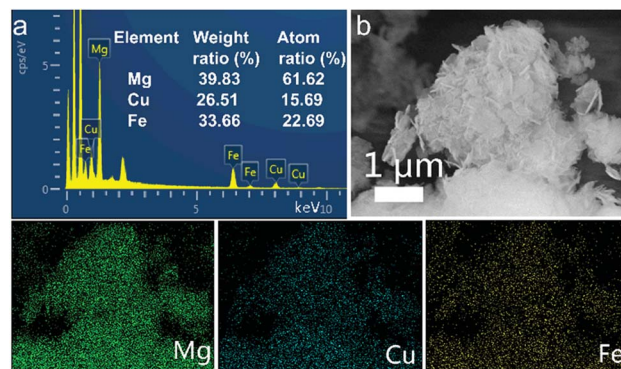
Fig. 5 (a) EDX spectrum of MgCuFe-LDH; (b) elemental mapping of MgCuFe-LDH for Mg, Cu and Fe.
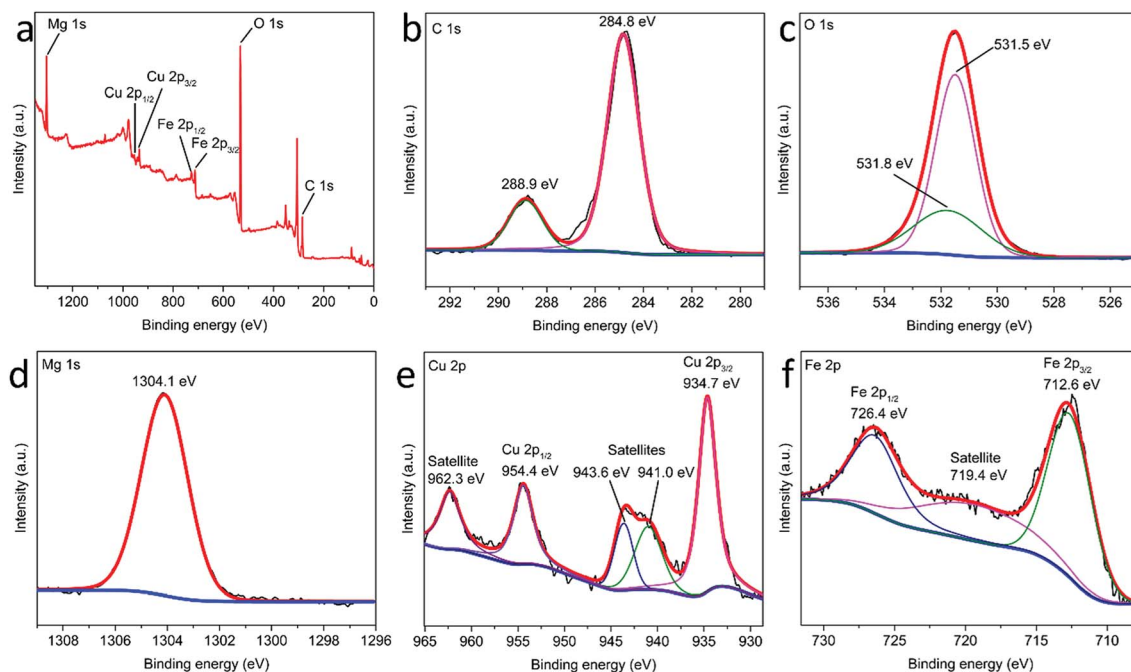
Fig. 6 (a) Full XPS spectrum of MgCuFe-LDH and high-resolution XPS spectra of (b) C 1s, (c) O 1s, (d) Mg 1s, (e) Cu 2p and (f) Fe 2p.

spectrum of O 1s is consisted of two peaks (Fig. 6c), and the binding energy at 531.5 eV can be attributed to the hydroxyl ions in LDH, the binding energy at 531.8 eV can be associated with the carbonate groups. In Fig. 6d, the peak at 1304.1 eV is indicative of Mg 1s. The high-resolution XPS spectrum of Cu 2p displays two strong peaks at 934.7 and 954.4 eV, which can be ascribed to Cu $2p_{3/2}$ and Cu $2p_{1/2}$, respectively (Fig. 6e). Additionally, three satellite peaks at 941.0, 943.6 and 962.3 eV could be observed. These results imply that Cu existed as Cu(II) in MgCuFe-LDH.[31–37] In the high-resolution XPS Fe 2p spectrum (Fig. 6f), two apparent peaks appeared at 712.6 eV for Fe $2p_{3/2}$ and 726.4 eV for Fe $2p_{1/2}$, with a satellite peak at 719.4 eV, which is the characteristic of Fe(III).[38,39]

3.2 Catalytic performance of MgCuFe-LDH in PMS activation for organic pollutants degradation

3.2.1 Catalytic performance for acetaminophen degradation. In order to explore the contributions of Cu and Fe in LDH

to PMS activation, the catalytic performances of MgFe-LDH, MgCuAl-LDH and MgCuFe-LDH for acetaminophen degradation were investigated (Fig. 7a). After a reaction of 20 min, 36.6%, 61.3% and 92.8% of acetaminophen were degraded by MgFe-LDH, MgCuAl-LDH and MgCuFe-LDH, respectively. The physical adsorption of acetaminophen on all the three LDH materials is negligible. From Fig. 7b, it can be seen that the degradation process of acetaminophen by PMS/LDH is fitted well with the first-order reaction. The reaction rate constants were 0.0218 min^{-1} ($R^2 = 0.990$), 0.0450 min^{-1} ($R^2 = 0.986$) and 0.1324 min^{-1} ($R^2 = 0.995$) for MgFe-LDH, MgCuAl-LDH and MgCuFe-LDH, respectively. The results suggest that both Cu and Fe played critical roles in acetaminophen degradation. Furthermore, the Cu and Fe of MgCuFe-LDH showed synergistic effect in PMS activation for acetaminophen degradation.

Fig. 8a displays the influence of catalyst loading on PMS activation for acetaminophen degradation. As well known, increasing catalyst loading can provide more active sites to react with PMS, and thus remarkably facilitate the production of reactive species. It can be easily observed that 62.3% of acetaminophen was degraded in 20 min at 0.1 g L^{-1} catalyst, while above 92.0% acetaminophen degradation was achieved in 20 and 15 min when the catalyst loading was 0.3 and 0.4 g L^{-1}, respectively. Without any catalyst, PMS itself could hardly degrade acetaminophen and no more than 4.0% of acetaminophen was removed in 25 min.

Acetaminophen removal efficiency in PMS/MgCuFe-LDH system is also affected by PMS dosage, as presented in Fig. 8b. The degradation efficiency increased from 83.3% to 96.3% and from 89.1% to 97.6% with the addition of PMS from 0.2 to 1.0 mM after a reaction time of 15 and 25 min, respectively. Moreover, the physical adsorption of acetaminophen on MgCuFe-LDH is negligible.
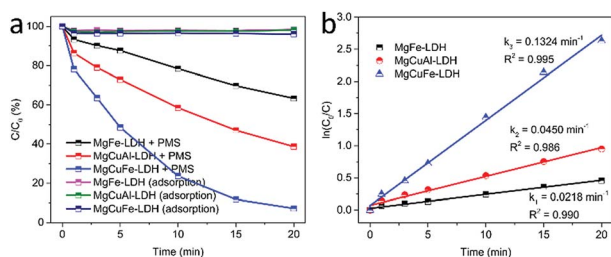

Fig. 7 (a) Catalytic performances of different LDH materials in PMS activation for acetaminophen degradation; (b) first-order kinetic plots for degradation of acetaminophen by different LDH materials. Reaction conditions: [acetaminophen] = 5 mg L^{-1}, [PMS] = 0.5 mM, [LDH] = 0.3 g L^{-1}, T = 25 °C, initial solution pH = 6.0.
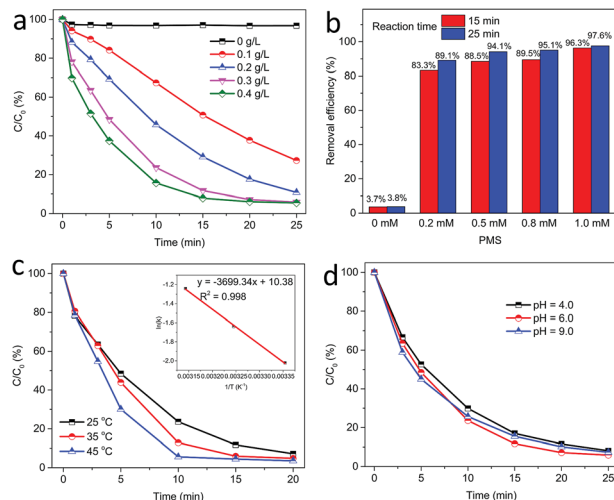
Fig. 8 Effects of (a) catalyst loading, (b) PMS dosage, (c) reaction temperature and (d) initial solution pH on acetaminophen degradation efficiency in PMS/MgCuFe-LDH system. Reaction conditions: [acetaminophen] = 5 mg L^{-1}, [PMS] = 0.5 mM (for a, c and d)), [MgCuFe-LDH] = 0.3 g L^{-1} (for b, c and d)), T = 25 °C (for a, b and d)), initial solution pH = 6.0 (for a, b and c)).

The effect of reaction temperature on acetaminophen degradation in PMS/MgCuFe-LDH system is given in Fig. 8c. The degradation efficiency of acetaminophen has a relatively obvious change at varying temperature. Above 92.8% of acetaminophen could be degraded at 10, 15 and 20 min, corresponding 45, 35 and 25 °C, respectively. The enhanced degradation efficiency of acetaminophen at high temperatures can be attributed to the acceleration of reactive species production due to the endothermic nature of PMS activation process, consistent with previous reports.[10,40,41] Reaction rate constants (k) at different reaction temperatures can be obtained based on first-order kinetics. The reaction rate constants were 0.2890, 0.1940 and 0.1324 min^{-1} at 45, 35 and 25 °C, respectively. The activation energy (E_a) was calculated using the Arrhenius equation (eqn (1)). Based on the relationship between the reaction rate constants and the reaction temperature (inset of Fig. 8c), the activation energy was 30.8 kJ mol^{-1}.

$$\ln(k) = \ln(A) - \frac{E_a}{R}\frac{1}{T} \qquad (1)$$

where k is the reaction rate constant, A is the pre-exponential factor, E_a is the activation energy, R is the universal gas constant and T is the absolute temperature (in kelvins).

The effect of initial solution pH on acetaminophen degradation efficiency in PMS/MgCuFe-LDH system was studied. The initial solution pH was adjusted using 0.1 M HNO$_3$ and 0.1 M NaOH. Fig. 8d shows that the catalytic activity of MgCuFe-LDH was slightly affected by pH over the range of 4.0–9.0. In the studied pH range, above 91.0% of acetaminophen could be degraded at 25 min. The result suggests that MgCuFe-LDH possesses high catalytic activity in PMS activation for organic pollutants degradation in the pH range 4.0–9.0.

TOC analysis was used to investigate the mineralization of organic contaminants in the catalytic oxidation process. It can
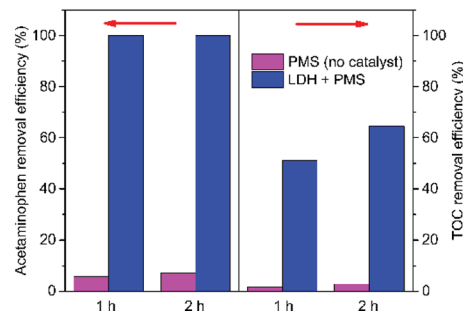

Fig. 9 Catalytic performance of MgCuFe-LDH in PMS activation for acetaminophen and TOC removal. Reaction conditions: [acetaminophen] = 5 mg L^{-1}, [MgCuFe-LDH] = 0.3 g L^{-1}, [PMS] = 2 mM, T = 25 °C, initial solution pH = 6.0.

be observed from Fig. 9 that the TOC removal efficiency was much lower than the acetaminophen removal efficiency. Acetaminophen could be completely degraded within 1 h in the PMS/LDH system, while the removal efficiency of TOC was only 64.5% even after 2 h. From Fig. 9, it can be seen that the removal efficiencies of both acetaminophen and TOC were very low by PMS (no catalyst).

3.2.2 Catalytic performance for RhB decolorization. The catalytic performance of MgCuFe-LDH was also investigated for decolorization of RhB. Fig. 10 exhibits that PMS could slightly decolorize RhB and only 13.5% of RhB was decolorized in 45 min. The physical adsorption of RhB on MgCuFe-LDH is also very limited. However, RhB was almost completely decolorized (99.5%) in PMS/MgCuFe-LDH system within 45 min and the inset of Fig. 10 shows the colour photographs of RhB solution before and after reaction. Compared with the previously reported CuFe-oxide catalysts, MgCuFe-LDH shows moderate catalytic performance for organic pollutants (acetaminophen and RhB) degradation (Table S1†).

3.2.3 Catalytic performance in actual water samples. In order to assess the catalytic performance of MgCuFe-LDH in actual water body, the experiments in the water samples of Taihu Lake spiked with acetaminophen (2 mg L^{-1}) or RhB
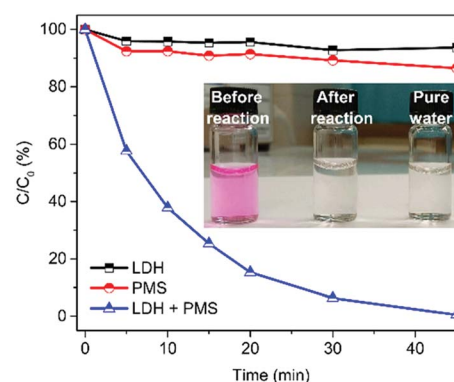

Fig. 10 Catalytic performance of MgCuFe-LDH in PMS activation for decolorization of RhB. Reaction conditions: [RhB] = 5 mg L^{-1}, [MgCuFe-LDH] = 0.3 g L^{-1}, [PMS] = 0.5 mM, T = 25 °C, initial solution pH = 5.2.
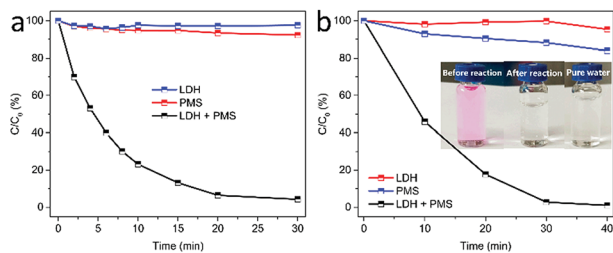
Fig. 11 Catalytic performance of MgCuFe-LDH in PMS activation for degradation of (a) acetaminophen and (b) RhB in actual water samples. Reaction conditions: [acetaminophen or RhB] = 2 mg L^{-1}, [MgCuFe-LDH] = 0.3 g L^{-1}, [PMS] = 0.5 mM, T = 25 °C, initial pH of acetaminophen solution = 8.0, initial pH of RhB solution = 7.9.

(2 mg L^{-1}) were carried out. The relative parameters of Taihu Lake water are as follows: pH = 8.1, chemical oxygen demand = 4.9 mg L^{-1}, turbidity = 45.4 NTU, dissolved oxygen = 6.9 mg L^{-1}, ammonia nitrogen = 0.14 mg L^{-1}. As seen from Fig. 11, acetaminophen and RhB in the actual water samples can be effectively degraded by MgCuFe-LDH in the presence of PMS, highlighting the practicability of MgCuFe-LDH in water remediation.

3.2.4 Stability and reusability of MgCuFe-LDH. The stability and reusability of MgCuFe-LDH were evaluated. The concentrations of leaching metal ions during degradation process are presented in Fig. 12a. During the entire degradation process, there was no detectable iron ion. While along with the reaction, the concentrations of copper ion and magnesium ion gradually increased. The concentrations of copper ion and magnesium ion reached 0.77 and 4.98 mg L^{-1} at 30 min, respectively. The reusability of MgCuFe-LDH is shown in Fig. 12b. After 30 min of reaction, MgCuFe-LDH was recovered

by filtration, washed with ultrapure water for three times and then re-dispersed in acetaminophen solution for next experiment. It can be seen from Fig. 12b that the catalytic activity of MgCuFe-LDH had almost no loss in the four successive experimental runs. The concentrations of leaching metal ions in PMS/MgCuFe-LDH system after different cycles were also detected. As shown in Fig. 12c, the concentrations of copper ion and magnesium ion increased with the increase of the number of cycles. However, iron ion was not detected in the four successive experimental runs. Additionally, the metal molar ratios of MgCuFe-LDH before and after three consecutive runs also confirmed the leaching of metal species from LDH (Table 1). The XRD patterns of MgCuFe-LDH before and after three consecutive runs showed minor differences (Fig. 12d). The differences may result from the leaching of metal species from LDH material.

3.3 Catalytic mechanism of PMS activation on MgCuFe-LDH

To disclose the activation mechanism on MgCuFe-LDH, the involved radicals generated during the PMS activation process were investigated through radical scavenger experiments. *tert*-Butanol and ethanol were used as the scavengers of hydroxyl radicals (·OH) and SO$_4$$^{•-}$/·OH radicals, respectively.[42,43] Fig. 13a shows the effects of *tert*-butanol and ethanol on acetaminophen catalytic degradation in PMS/MgCuFe-LDH system. When 250 mM of ethanol was added to reaction solution, the degradation efficiency of acetaminophen obviously declined from 94.1% to 72.8% at 25 min. The degradation efficiency of acetaminophen decreased with the increase of ethanol in reaction solution. As compared with ethanol, *tert*-butanol in solution has a lesser effect on acetaminophen degradation. The quenching effects from *tert*-butanol and ethanol indicate that both SO$_4$$^{•-}$ and ·OH are responsible for the oxidation process.

EPR was used to further probe the generation of reactive radicals. Fig. 13b reveals that both SO$_4$$^{•-}$ and ·OH are involved as the main reactive radicals during PMS activation using MgCuFe-LDH as the catalyst.[44,45] In addition, the signals of both DMPO–SO$_4$$^{•-}$ adduct and DMPO–·OH adduct were not detected in the absence of MgCuFe-LDH. These results suggest that MgCuFe-LDH is a promising material to activate PMS for organic pollutants degradation.
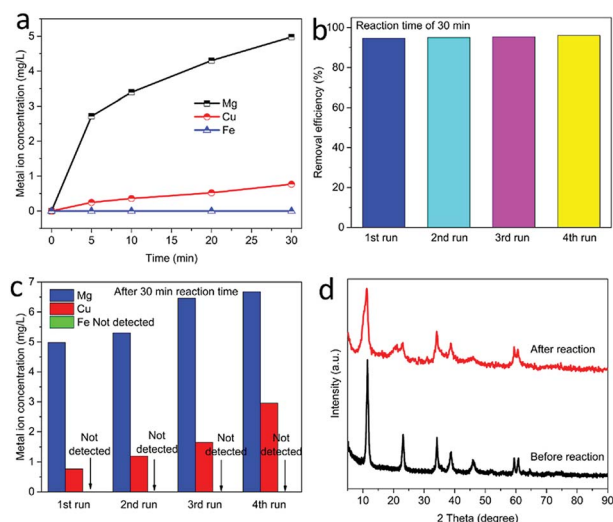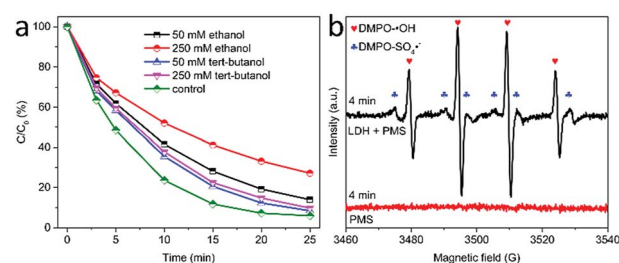

Fig. 12 (a) Concentrations of leaching metal ions during degradation process; (b) cycling test of MgCuFe-LDH for acetaminophen removal by activation of PMS; (c) concentrations of leaching metal ions after different cycles in PMS/MgCuFe-LDH system; (d) XRD patterns of MgCuFe-LDH before and after three consecutive runs. Reaction conditions: [acetaminophen] = 5 mg L^{-1}, [MgCuFe-LDH] = 0.3 g L^{-1}, [PMS] = 0.5 mM, T = 25 °C, initial solution pH = 6.0.

Fig. 13 (a) Effects of radical scavengers on acetaminophen degradation in PMS/MgCuFe-LDH system; (b) EPR spectra of PMS activation with or without MgCuFe-LDH. Reaction conditions: [acetaminophen] = 5 mg L^{-1}, [MgCuFe-LDH] = 0.3 g L^{-1}, [PMS] = 0.5 mM, T = 25 °C, initial solution pH = 6.0, [DMPO] = 40 mM (for (b)).
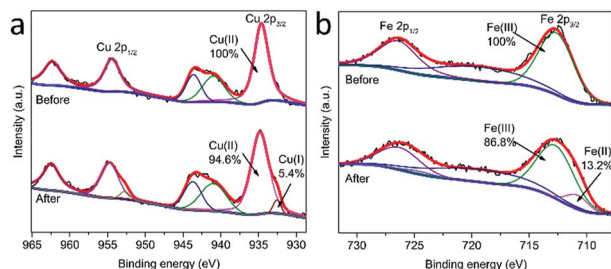
Fig. 14 High-resolution XPS spectra of (a) Cu 2p and (b) Fe 2p of MgCuFe-LDH before and after three consecutive runs. Reaction conditions: [acetaminophen] = 5 mg L^{-1}, [MgCuFe-LDH] = 0.3 g L^{-1}, [PMS] = 0.5 mM, T = 25 °C, initial solution pH = 6.0.

In order to further explore the activation mechanism of PMS on MgCuFe-LDH, XPS was used for determining the chemical states of surface Cu and Fe. Fig. 14 gives the high-resolution XPS Cu 2p and Fe 2p spectra of MgCuFe-LDH before and after the reaction. After the catalytic reaction, 5.4% of the total Cu was transformed from Cu(II) to Cu(I), while 13.2% of the total Fe was transformed from Fe(III) to Fe(II). Based on the results, we propose that the Cu(II)–Cu(I) and Fe(III)–Fe(II) redox processes are involved in PMS activation.

According to the above analysis, the possible mechanism of PMS activation on MgCuFe-LDH for the degradation of aqueous organic pollutants could be proposed as follows (Fig. 15). First, Cu(II)/Fe(III) in MgCuFe-LDH could activate PMS to produce SO$_5$$^{\bullet-}$ radicals through eqn (2) and (3) with themselves reduce to Cu(I)/Fe(II). Second, the generated Cu(I)/Fe(II) could be quickly oxidized by PMS to produce Cu(II)/Fe(III) and SO$_4$$^{\bullet-}$ radicals (eqn (4) and (5)), which makes the reaction proceed circularly until PMS is entirely consumed. In the process, $\cdot$OH is generated through the reaction between SO$_4$$^{\bullet-}$ and OH$^-$/H$_2$O (eqn (6) and (7)).[46] In addition, Cu(I) could reduce Fe(III) to Fe(II) (eqn (8)).[8] The generated SO$_4$$^{\bullet-}$ radicals (E_0 = 2.5–3.1 V) and $\cdot$OH radicals (E_0 = 1.8–2.7 V) can react with organic pollutants rapidly due to their high redox potentials (eqn (9)).[47] Furthermore, the generated SO$_5$$^{\bullet-}$ radicals (E_0 = 1.1 V) may also play a role in the degradation of organic pollutants (eqn (9)).[47]
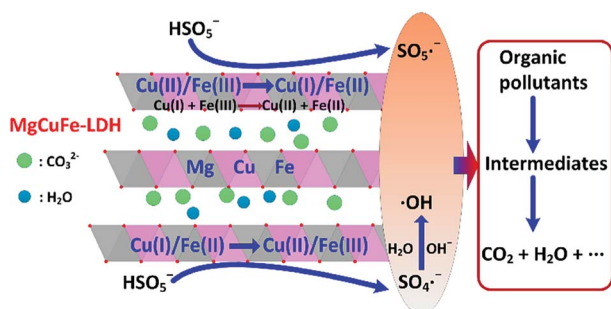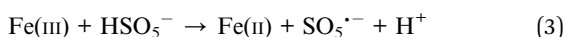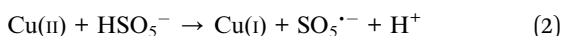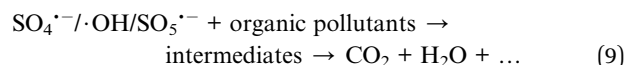
$$Cu(II) + HSO_5^- \rightarrow Cu(I) + SO_5^{\bullet-} + H^+ \qquad (2)$$

$$Fe(III) + HSO_5^- \rightarrow Fe(II) + SO_5^{\bullet-} + H^+ \qquad (3)$$

Fig. 15 Proposed mechanism of PMS activation on MgCuFe-LDH for aqueous organic pollutants degradation.

$$Cu(I) + HSO_5^- \rightarrow Cu(II) + SO_4^{\bullet-} + OH^- \qquad (4)$$

$$Fe(II) + HSO_5^- \rightarrow Fe(III) + SO_4^{\bullet-} + OH^- \qquad (5)$$
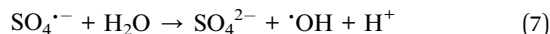
$$SO_4^{\bullet-} + OH^- \rightarrow SO_4^{2-} + {}^{\bullet}OH \qquad (6)$$

$$SO_4^{\bullet-} + H_2O \rightarrow SO_4^{2-} + {}^{\bullet}OH + H^+ \qquad (7)$$

$$Fe(III) + Cu(I) \rightarrow Fe(II) + Cu(II) \qquad (8)$$

$$SO_4^{\bullet-}/\cdot OH/SO_5^{\bullet-} + \text{organic pollutants} \rightarrow$$
$$\text{intermediates} \rightarrow CO_2 + H_2O + \dots \qquad (9)$$

4. Conclusions

In summary, MgCuFe-LDH was synthesized and successfully used as a catalyst for the first time to activate PMS for organic pollutants degradation. Compared with both MgFe-LDH and MgCuAl-LDH, MgCuFe-LDH exhibited significantly higher catalytic activity to activate PMS for acetaminophen degradation. Acetaminophen (5 mg L^{-1}) degradation at about 93.0% was achieved at 20 min by using 0.3 g L^{-1} MgCuFe-LDH and 0.5 mM PMS. Under the same conditions, RhB (5 mg L^{-1}) can be almost completely decolorized (99.5%) within 45 min. The activation energy (E_a) calculated with the Arrhenius equation was 30.8 kJ mol^{-1}. Radical scavenger and EPR experiments showed that SO$_4$$^{\bullet-}$ and $\cdot$OH existed in PMS/MgCuFe-LDH system. The generated radicals played vital roles in the catalytic degradation of organic pollutants. Moreover, a possible activation mechanism of PMS on MgCuFe-LDH was proposed. This study demonstrates that MgCuFe-LDH is a promising catalyst to activate PMS for the efficient degradation of organic pollutants in aqueous solutions.
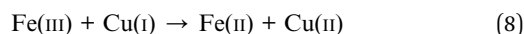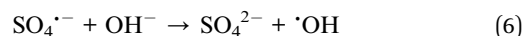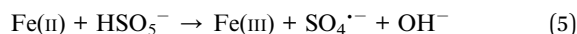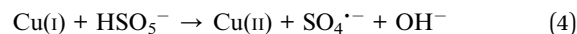
Conflicts of interest

There are no conflicts to declare.

Acknowledgements

References

1 X. Chen, W.-D. Oh, Z.-T. Hu, Y.-M. Sun, R. D. Webster, S.-Z. Li and T.-T. Lim, *Appl. Catal., B*, 2018, **225**, 243–257.
2 C. Guan, J. Jiang, C. Luo, S. Pang, Y. Yang, Z. Wang, J. Ma, J. Yu and X. Zhao, *Chem. Eng. J.*, 2018, **337**, 40–50.
3 K.-Y. A. Lin, H.-K. Lai and S. Tong, *J. Colloid Interface Sci.*, 2018, **514**, 272–280.
4 P. Shao, X. Duan, J. Xu, J. Tian, W. Shi, S. Gao, M. Xu, F. Cui and S. Wang, *J. Hazard. Mater.*, 2017, **322**, 532–539.
5 Y. Yang, J. Jiang, X. Lu, J. Ma and Y. Liu, *Environ. Sci. Technol.*, 2015, **49**, 7330–7339.

6 G. P. Anipsitakis and D. D. Dionysiou, *Environ. Sci. Technol.*, 2004, **38**, 3705–3712.

7 J. Deng, S. Feng, K. Zhang, J. Li, H. Wang, T. Zhang and X. Ma, *Chem. Eng. J.*, 2017, **308**, 505–515.

8 Y. Ding, L. Zhu, N. Wang and H. Tang, *Appl. Catal., B*, 2013, **129**, 153–162.

9 N. Jaafarzadeh, F. Ghanbari and M. Ahmadi, *Chemosphere*, 2017, **169**, 568–576.

10 X. Li, Z. Wang, B. Zhang, A. I. Rykov, M. A. Ahmed and J. Wang, *Appl. Catal., B*, 2016, **181**, 788–799.

11 Y. Wang, H. Sun, H. M. Ang, M. O. Tade and S. Wang, *Appl. Catal., B*, 2015, **164**, 159–167.

12 Y. Yao, Y. Cai, F. Lu, F. Wei, X. Wang and S. Wang, *J. Hazard. Mater.*, 2014, **270**, 61–70.

13 T. Zhang, H. Zhu and J.-P. Croue, *Environ. Sci. Technol.*, 2013, **47**, 2784–2791.

14 Z. Gao, J. Wang, Z. Li, W. Yang, B. Wang, M. Hou, Y. He, Q. Liu, T. Mann, P. Yang, M. Zhang and L. Liu, *Chem. Mater.*, 2011, **23**, 3509–3516.

15 S. Liu, S. C. Lee, U. Patil, I. Shackery, S. Kang, K. Zhang, J. H. Park, K. Y. Chung and S. C. Jun, *J. Mater. Chem. A*, 2017, **5**, 1043–1049.

16 M. Sarfraz and I. Shakir, *Journal of Energy Storage*, 2017, **13**, 103–122.

17 L. Wang, D. Wang, X. Y. Dong, Z. J. Zhang, X. F. Pei, X. J. Chen, B. Chen and J. Jin, *Chem. Commun.*, 2011, **47**, 3556–3558.

18 K.-H. Goh, T.-T. Lim and Z. Dong, *Water Res.*, 2008, **42**, 1343–1368.

19 Y. Guo, Z. Zhu, Y. Qiu and J. Zhao, *J. Environ. Sci.*, 2013, **25**, 944–953.

20 H. Lu, Z. Zhu, H. Zhang, J. Zhu and Y. Qiu, *Chem. Eng. J.*, 2015, **276**, 365–375.

21 Y. Lu, B. Jiang, L. Fang, F. Ling, J. Gao, F. Wu and X. Zhang, *Chemosphere*, 2016, **152**, 415–422.

22 G. Fan, F. Li, D. G. Evans and X. Duan, *Chem. Soc. Rev.*, 2014, **43**, 7040–7066.

23 H. Lu, Z. Zhu, H. Zhang, J. Zhu, Y. Qiu, L. Zhu and S. Kueppers, *ACS Appl. Mater. Interfaces*, 2016, **8**, 25343–25352.

24 X. Zhang, Z. Wang, N. Qiao, S. Qu and Z. Hao, *ACS Catal.*, 2014, **4**, 1500–1510.

25 J. Zhu, Z. Zhu, H. Zhang, H. Lu, Y. Qiu, L. Zhu and S. Kueppers, *J. Colloid Interface Sci.*, 2016, **481**, 144–157.

26 J. Zhu, Z. Zhu, H. Zhang, H. Lu, W. Zhang, Y. Qiu, L. Zhu and S. Kueppers, *Appl. Catal., B*, 2018, **225**, 550–562.

27 J. Zhu, Z. Zhu, W. Hu, H. Zhang, H. Lu and Y. Qiu, *Fresenius Environ. Bull.*, 2016, **25**, 2079–2089.

28 S. Aisawa, H. Hirahara, K. Ishiyama, W. Ogasawara, Y. Umetsu and E. Narita, *J. Solid State Chem.*, 2003, **174**, 342–348.

29 J. Zhao, J. Chen, S. Xu, M. Shao, Q. Zhang, F. Wei, J. Ma, M. Wei, D. G. Evans and X. Duan, *Adv. Funct. Mater.*, 2014, **24**, 2938–2946.

30 C. Lei, X. Zhu, B. Zhu, C. Jiang, Y. Le and J. Yu, *J. Hazard. Mater.*, 2017, **321**, 801–811.

31 H. Cheng, M.-L. Li, C.-Y. Su, N. Li and Z.-Q. Liu, *Adv. Funct. Mater.*, 2017, **27**, 1701833.

32 W. Guo, W. Sun and Y. Wang, *ACS Nano*, 2015, **9**, 11462–11471.

33 K. S. Joya and H. J. M. de Groot, *ACS Catal.*, 2016, **6**, 1768–1771.

34 M. Kuang, Q. Wang, P. Han and G. Zheng, *Adv. Energy Mater.*, 2017, **7**, 1700193.

35 L. Xie, C. Tang, K. Wang, G. Du, A. M. Asiri and X. Sun, *Small*, 2017, **13**, 1602755.

36 M. Yin, C. K. Wu, Y. B. Lou, C. Burda, J. T. Koberstein, Y. M. Zhu and S. O'Brien, *J. Am. Chem. Soc.*, 2005, **127**, 9506–9511.

37 F. Yu, F. Li, B. Zhang, H. Li and L. Sun, *ACS Catal.*, 2015, **5**, 627–630.

38 X. Lei, Z. Ye, N. Zhao, F. Lei and H. Yang, *Chem.–Eur. J.*, 2017, **23**, 17592–17597.

39 S. Liu, L. Zheng, P. Yu, S. Han and X. Fang, *Adv. Funct. Mater.*, 2016, **26**, 3331–3339.

40 R. Luo, C. Liu, J. Li, C. Wang, X. Sun, J. Shen, W. Han and L. Wang, *J. Mater. Chem. A*, 2018, **6**, 3454–3461.

41 R. Luo, C. Liu, J. Li, J. Wang, X. Hu, X. Sun, J. Shen, W. Han and L. Wang, *J. Hazard. Mater.*, 2017, **329**, 92–101.

42 X. Duan, K. O'Donnell, H. Sun, Y. Wang and S. Wang, *Small*, 2015, **11**, 3036–3044.

43 P. Shukla, S. Wang, K. Singh, H. M. Ang and M. O. Tade, *Appl. Catal., B*, 2010, **99**, 163–169.

44 X. Duan, H. Sun, Y. Wang, J. Kang and S. Wang, *ACS Catal.*, 2015, **5**, 553–559.

45 Y. Wang, C. Liu, Y. Zhang, W. Meng, B. Yu, S. Pu, D. Yuan, F. Qi, B. Xu and W. Chu, *Appl. Catal., B*, 2018, **235**, 264–273.

46 G.-X. Huang, C.-Y. Wang, C.-W. Yang, P.-C. Guo and H.-Q. Yu, *Environ. Sci. Technol.*, 2017, **51**, 12611–12618.

47 G. P. Anipsitakis and D. D. Dionysiou, *Environ. Sci. Technol.*, 2003, **37**, 4790–4797.